PERGAMON

Micron 30 (1999) 41–49

micron

Structural investigations of metal–semiconductor surfaces

D. Grozea[a,*], E. Landree[a], C. Collazo-Davila[a], E. Bengu[a], R. Plass[b], L.D. Marks[a]

[a]*Department of Materials Science and Engineering, Northwestern University, Evanston, IL 60208, USA*
[b]*Department of Physics, University of Wisconsin-Milwaukee, Milwaukee, WI 53201, USA*

Received 21 January 1998; received in revised form 8 June 1998; accepted 9 June 1998

Abstract

A complete understanding of surface phenomena in electronic materials requires knowledge of the atomic arrangement. Recent results for surface atomic structures using high resolution transmission electron microscopy and transmission electron diffraction are presented. These results include atomic level imaging of complex structures such as Si(1 1 1)-(7 × 7) showing not just the adatoms but also the buried dimers, and accurate refinements of surface models based on electron diffraction data. A new concept for surface phases is reviewed, replacing the typical simple diagrams showing the temperature versus coverage regime with a phase diagram obeying Gibbs phase rules (for the system Au on Si(1 1 1), submonolayer regime). Another important development, Direct Methods, constitutes a new technique to find an initial estimate for the refinement of surface atomic models. Using a Minimum Relative Entropy method, the Direct Methods approach was successful for the case of transmission electron as well as X-ray diffraction data. Its application to solving a number of surface reconstructions is discussed.

Keywords: Semiconductors; Surface reconstruction; TED; HREM; Direct Methods; Minimum Relative Entropy; Phase maps; Computer simulations; χ^2 minimization

1. Introduction

The importance of surface and thin-film science has been steadily increasing and now constitutes one of the most significant aspects of the semiconductor industry. Despite this practical importance, fundamental understanding of surface and interface phenomena has been difficult to attain owing to their complexity, and progress has often been made through trial-and-error empirical approaches. More often than not uncontrolled impurities at surfaces as well as interdiffusion or reactions determine the macroscopic scale properties of the semiconductor devices.

In many cases atoms from the surface layer of a crystal do not occupy the positions that would be expected from a simple continuation of the bulk structure. The bonding configuration of the surface atoms being different from that of the bulk atoms, small shifts in atom positions either normal to or parallel to the crystal surface can lead to a substantial increase in bonding energy and a lowering of the total energy of the system. This new atomic configuration, called a reconstruction, can extend several atomic layers into the bulk. In addition to native reconstructions, the presence of adsorbate atoms on the surface, usually less than one monolayer, induces many different surface reconstructions. These can be considered as the early stages of nucleation and thin film growth on that particular substrate.

A standard notation for reconstructions is M(*hkl*)-($n \times m$)RΦ-C where M(*hkl*) is the bulk material and its crystallographic orientation (Wood, 1964). Considering that **a** and **b** are the two-dimensional surface unit vectors describing the original surface periodicity, ($n \times m$) indicates the new surface structure with a periodicity n times along the original **a** unit cell direction and m times along the **b** direction. If the reconstruction lattice is rotated with respect to the original surface unit cell, an RΦ notation is used to define the rotation angle Φ. Finally, an adsorbate induced reconstruction is indicated by its chemical symbol C.

Despite the development of numerous experimental techniques and advances in theoretical calculations, in most cases the atomic surface structure is not yet unambiguously known. More than once a structure has been believed to be solved and reconsidered in later studies (see, for example, the case of the Si(1 1 1)-(3 × 1)Ag surface, Weitering et al., 1994; Erwin, 1995; Collazo-Davila et al., 1998a). At the moment there are no techniques which can straightforwardly image the atomic arrangement at the surface. Scanning tunneling microscopy (STM) images show the density of surface states, not atom locations (e.g. Binning and

* Corresponding author. Tel.: + 1-847-491-3267; fax: + 1-847-491-7820.
E-mail address: dgrozea@merle.acns.nwu.edu (D. Grozea)

0968–4328/99/$ - see front matter
PII: S0968-4328(98)00039-0

Rohrer, 1987). A protruding atom or a high density of states have the same effect leading to an intricate interpretation of results. Moreover, STM is sensitive to only the outermost layer of atoms ignoring subsurface relaxation. This limitation does not apply to transmission electron microscopy (TEM) and X-ray diffraction. High resolution transmission electron microscopy (HREM) can provide detailed atomic scale information about surface structures by direct imaging. This approach has been successful in resolving not only heavy atoms such as Ir on Ir(1 0 0)-5 × 1 surface (Marks et al., 1993) and Au atoms on Si(1 1 1)-5 × 2 (Marks and Plass, 1995), but also lighter atoms such as all the Si atoms from the Si(1 1 1)-(7 × 7) structure (Bengu et al., 1996). However, HREM information is tedious to acquire and the signal to noise ratio is extremely low.

On the other hand, the use of diffraction techniques, electron and X-ray alike, to investigate the surface atomic arrangement necessitates a starting model close to the correct structure. This approach has the advantage of easy and accurate refinement. Patterson maps generated from surface diffraction data constitute a technique to solve the surface atomic geometry (see, for instance, Woolfson and Fan, 1995). These maps show positive peaks corresponding to interatomic vectors. Therefore, the map analysis could lead to information on only some part of the structure as a result of the difficulty of picking out many individual vectors and the presence of artifacts, as well as false peaks induced by special relationships between interatomic vectors.

More powerful than the Patterson approach, Direct Methods have become a routine analysis technique for solving bulk crystal structure from X-ray (see, for example, Giacovazzo, 1980; Woolfson, 1987; Woolfson and Fan, 1995) and from electron diffraction data (not so routine, Dorset, 1995). Direct Phasing Methods have been recently applied by our group with success to surface diffraction data to determine the initial structure estimate. This approach has worked for electron as well as X-ray diffraction data, since a necessary condition, kinematical data, is an adequate approximation in both cases (Tanishiro and Takayanagi, 1989a,b). The application of Direct Methods to known reconstructions found successfully in each case the ''correct'' solution: Si(1 1 1)-(7×7) (Gilmore et al., 1997), Si(1 1 1)-($\sqrt{3}\times\sqrt{3}$)R30°Au and Si(1 1 1)-(5×2)Au (Marks et al., 1997) (using electron data in every case). Subsequently, a large array of unknown structures were tackled for either electron or X-ray data, on semiconductor surfaces: Si(1 1 1)-(4×1)In (Collazo-Davila et al., 1997b), Si(1 1 1)-(6×6)Au (Marks et al., 1998b), Si(1 1 1)-(3×1)Ag (Collazo-Davila et al., 1998a), Ge(1 1 1)- (4×4)Ag (Collazo-Davila et al., 1998b), and metal oxides: TiO_{2-x}(1 0 0)-(1×3) (Landree et al., 1998), MgO(1 1 1)-($n\sqrt{3}$) (Plass et al., 1998).

In this article, we will describe several techniques, HREM, transmission electron diffraction (TED), and heavy-atom holography, and review recently obtained results on metal-semiconductor surfaces. Following this, the Direct Methods approach and its application to solving a number of surface structures using surface X-ray or TED data will be presented.

2. High resolution electron microscopy

A strong point of the HREM technique is its ability to look at both the surface and the bulk at the same time, as surface reconstructions often involve relaxation of the top several layers near the surface. However, the atomic or almost-atomic resolution may be limited in practice because the surface-specific information appears as a weak signal either buried in noise or on top of a large background.

Considering the orientation of the specimen surface with respect to the incident electron beam, two imaging modes of HREM of surfaces can be discussed: profile view (Marks and Smith, 1983) or plan view imaging. In the case of profile imaging mode, the electron beam is parallel to the surface. Although applied with success in several cases, e.g. the study of Au(1 1 0)-(2 × 1) reconstruction (Marks, 1983) or CdTe(0 0 1)-(2 × 1) and (3 × 1) surfaces (Lu and Smith, 1991), this technique does not image individual atoms but only arrangements of the atomic rows parallel to the beam. Other limitations arise because of the very thin edge involved. This mode's application to large surface structures is therefore limited. Another limitation is related to obtaining an equilibrium surface configuration given the intrinsic thermodynamical instability of a thin profile edge.

In the other mode, plan view imaging, the incident beam is perpendicular to the surface of interest. Thermodynamical instability is no longer a problem in this case. Information from both surfaces, top and bottom, and the bulk material in-between is present in images. Plan view imaging can be performed in either on-zone axis mode (Krakow, 1982; Nihoul et al., 1984; Xu et al., 1993), where the electron beam is parallel to a major zone axis of the material, or off-zone axis mode (Marks et al., 1993; Marks and Plass, 1995) by tilting the crystal away from the principal axial orientation. The surface structure can be approximated as almost two-dimensional and therefore it gives rise to a set of continuous lines in reciprocal space (rel rods) in contrast to the sets of sharp maxima at the reciprocal lattice points due to the bulk. The latter are only slightly elongated in the direction parallel to the incident beam. Thus, with tilting off the zone axis the amplitudes of the reflections from the bulk lattice may be significantly reduced relative to the reflections from the surface layers (Xu and Marks, 1992). A higher surface sensitivity may be achieved by this modification of the imaging conditions reducing the bulk signal and leading to better HREM images.

The application of the off-zone imaging mode has been successful in identifying heavy atom positions, e.g. the case of Au sites in the Si(1 1 1)-(5 × 2)Au (or 5 × 2 Au hereafter) reconstruction (Marks and Plass, 1995). The images provided the starting elements necessary to solve the atomic arrangement of this surface. After noise filtering using a

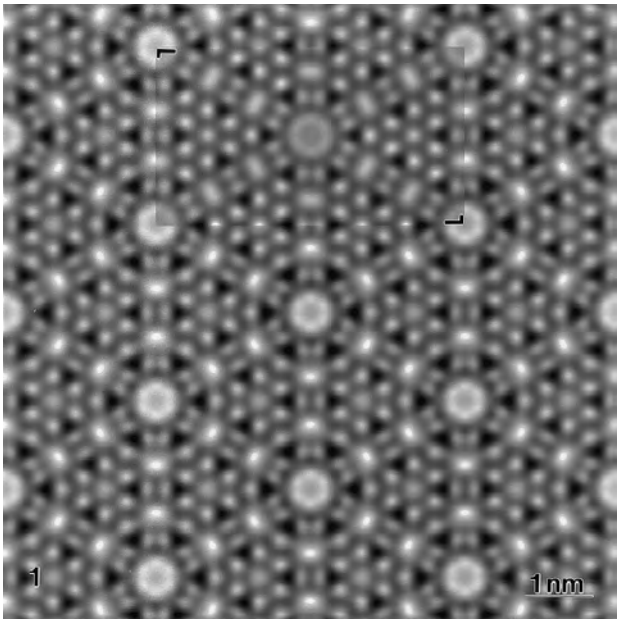

Fig. 1. High resolution electron microscopy image of Si(1 1 1)-(7 × 7) surface. The black ''dots'' correspond approximately to all the atoms in the first three layers. Inset in the image is a multislice calculation (top). Scale bar indicates 1 nm.

modified parametric Wiener filter (Marks, 1996), the HREM images showed two lines of strong scattering features that could be clearly identified as the Au atoms due to their stronger scattering characteristics as compared to the Si atoms. Also present in the images were weaker and less resolved features due to Si filled sites.

In fact a combination of diffraction and imaging techniques is typically necessary to fully characterizing a surface structure by TEM. Solving the 5 × 2 Au structure further involved the application of a heavy-atom holography method (Marks and Plass, 1995), later described in more detail in this article, which showed several possible Si sites requisite for the structure completion. The resulting models were finally refined against TED data using a χ^2 minimization analysis. For this final fitting procedure the bulk crystal and dynamical effects were taken into consideration.

An example of how powerful HREM imaging can be is the case of the Si(1 1 1)-(7 × 7) reconstruction. This is one of the most complicated known surface structures, involving a total of 102 atoms in the unit cell distributed in the top three layers. While STM images show only the structure's adatoms (first outmost layer) and corner holes, important parts of the model such as the dimers in the third layer are invisible to STM.

Starting from experimental HREM images obtained with a zone axis orientation, the image processing consisted of noise reduction and numerical inversion (the latter necessary due to another problem of plan view imaging, the separation of top and bottom surfaces) (Bengu et al., 1996). The image contrast was enhanced by the application of the Wiener filter already mentioned, which removed the shot noise without introducing any artifacts. Afterwards, the highly nonlinear bulk {2 2 0} beams were digitally removed, allowing only the surface reflections to contribute to the images; a valid case of the kinematical approximation with linear imaging. The recovery of a single surface from the two overlapping surface images was performed assuming p6mm symmetry and a Wiener filter. The resulting images show clearly the atomic scale surface structure at a resolution close to 2 Å revealing all the atoms in the top three layers including the dimers in the third layer (Fig. 1).

3. Transmission electron diffraction

The major difficulty in solving unknown surface structures based only on diffraction data is the lack of a starting point from which to refine atomic positions. However, if an initial model is known, information about the atomic structure of a reconstruction can be obtained from quantitative analysis of beam intensities in TED patterns. Electron diffraction patterns are recorded mostly in the off-zone axis mode as it yields better surface data as has already been discussed. Typically, a series of diffraction patterns are recorded at different exposure times to cover the large dynamic variation of surface and bulk beams. The experimental data sets are reduced through a cross-correlation technique developed by our group (Xu et al., 1994). To obtain the final atomic arrangement, either a kinematical or a dynamical approach including the effects of crystal thickness and tilt is used to numerically calculate the beam intensity generated from an initial structure model. The absolute intensities of the surface diffraction spots are calculated and then compared against the experimentally measured ones, and the difference is minimized in an iterative process to yield the final model.

For the native Ge surface reconstruction, Ge(0 0 1)-(2 × 1), the lateral atomic displacements for the first top six layers extending into the bulk have been determined (Collazo-Davila et al., 1997a). The simulations included dynamical refinements taking into account crystal thickness and tilt. The atomic positions coincide with the results from X-ray studies to within a few hundredths of an Ångstrom. Such a precise experimental agreement suggests the use of the Ge(0 0 1)-(2 × 1) surface as a valuable model system for theoretical studies of native surface reconstructions.

In the case of Si(1 1 1)-($\sqrt{3}\times\sqrt{3}$)R30°Au (or $\sqrt{3}\times\sqrt{3}$ Au hereafter) reconstruction, TED analysis revealed the average atomic structure and the possible nature of the surface domain walls (Plass and Marks, 1995). Three data sets were fitted individually or simultaneously to models found in the literature and variations of those. A final model was proposed with the first layer of the structure containing Au atoms forming slightly rotated trimers. The second layer of the structure consists of silicon trimers rotated also by a small angle about their centers. It is

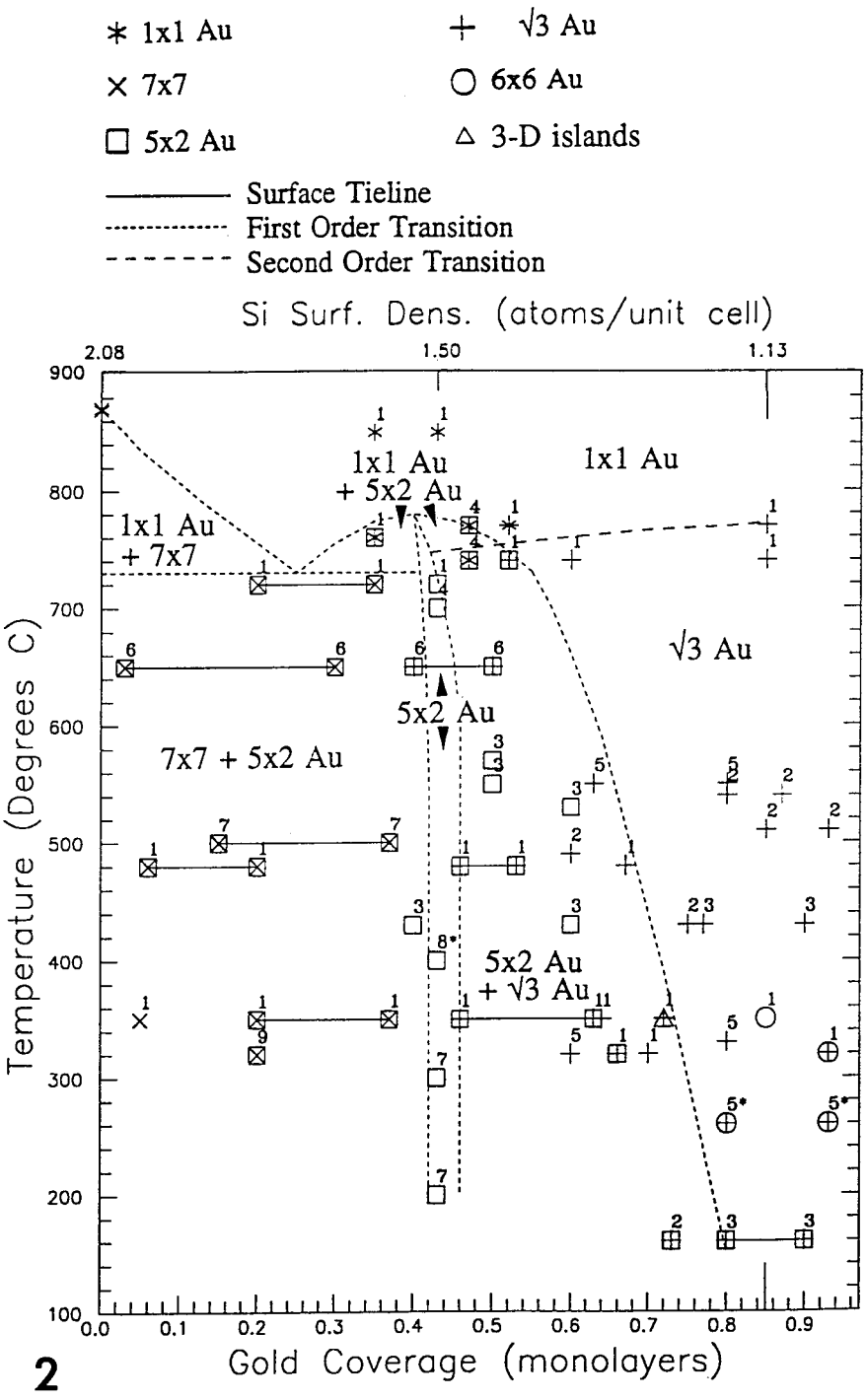

Fig. 2. Proposed submonolayer Au on Si(1 1 1) surface phase diagram showing in situ experimental results from the literature. The number over the symbols corresponds to a reference number, as follows 1: Ŝwiěch et al. (1991); 2: Yuhara et al. (1992a); 3: Yuhara et al. (1992b); 4: Diamon et al. (1990); 5: Takahashi et al. (1991); 6: Tanishiro and Takayanagi (1989b); 7: Hasegawa et al. (1991); Hasegawa et al. (1992); Hasegawa et al. (1996); 8: Minoda et al. (1992); 9: Shibata et al. (1992). Starred (*) reference numbers indicate that the coverage was estimated. Single symbols represent a reported surface completely covered by that symbol's surface structure. Overlapping symbols represent coexistence of the corresponding structures on the surface. Solid lines represent experimental tie lines between surfaces with mixed compositions. The short dashed curves are potential locations of first order phase transitions between different phase regions. The longer dashed curves represent a second order transition. Key: *, 1 × 1 Au; ×, 7 × 7; □, 5 × 2 Au; +, $\sqrt{3}\times\sqrt{3}$ Au; ○, 6 × 6 Au; △, 3-D Au islands.

worth mentioning that since TEM is not sensitive to displacements parallel to the electron beam, the *z* axis distance between the Au and Si layers could not be measured.

Solving the two main surface phases for Si(1 1 1)-Au in the submonolayer regime, the 5 × 2 Au and $\sqrt{3}\times\sqrt{3}$ Au reconstructions, in conjunction with results from numerous recent studies on this system, opened the way for a new approach to surface structure understanding. Instead of the

familiar phase map showing the temperature versus coverage regime for surface phases, a phase diagram obeying Gibbs phase rules, with phase boundaries based on thermodynamics principles is proposed (Plass and Marks, 1997). This includes redefining the reconstructions in terms of ''line compounds'' or ''surface solutions''. As both 5×2 Au and $\sqrt{3} \times \sqrt{3}$ Au phases can vary their Au content, they are considered surface solutions. Another assumption for a sound thermodynamics evaluation is that the studied system is closed with respect to the amount of its constituents, a reasonable approximation in the present case within a certain temperature range (100°C–900°C), coverage (under one monolayer), and length of time (tens of minutes). Fig. 2 shows the proposed submonolayer Au on Si(1 1 1) phase diagram with in situ experimental results from the literature. This complex phase diagram includes lower coverage eutectoid and higher coverage peritectoid regions, assuming the high temperature 1×1 Au and the $\sqrt{3} \times \sqrt{3}$ Au phases are related by a second order transition.

4. Direct Methods

Direct Phasing Methods were applied to find an initial estimate for the refinement of atomic models using a Minimum Relative Entropy method coupled with a genetic algorithm for global optimization (Landree et al., 1997; Marks and Landree, 1998; Marks et al., 1998a).

From diffraction techniques only beam intensities/moduli of the structure factors can be obtained. To restore the charge density or the scattering potential, in the X-ray or electron diffraction case respectively, the phases are also necessary. Direct Methods solve the diffraction phase problem using the probability relationships which exist between the intensities and the phases of the diffracted beams (Woolfson and Fan, 1995). This is achieved through a routine search of sets of phases for a given set of measured intensities which best satisfy these probability relationships. The solutions, sets of plausible phases ranked by some figure of merit (FOM), generate phase maps used to construct initial models of the atomic structure. Finally, the models are discriminated upon based on the comparison of the calculated and measured structure factors/beam intensities using in general a χ^2 minimization.

In the case of a structure with N non-overlapping identical atoms, a complete set of unitary structure factors $U(\mathbf{k})$ will satisfy the Sayre equation:

$$U(\mathbf{k}) = N \sum_h U(\mathbf{k} - \mathbf{h}) U(\mathbf{h}). \tag{1}$$

If some initial phases are known, the Sayre equation can be used to generate the missing phases via the Tangent Formula. The new phases are then fed back iteratively into the Sayre equation to restore all the missing phases and a self-consistency test is performed at each iteration. The process is not a true minimization but rather a successive approximation method similar to a Picard iteration, and Eq. (1) can be rewritten as:

$$U_{n+1}(\mathbf{k}) = N \sum_h U_n(\mathbf{k} - \mathbf{h}) U_n(\mathbf{h}), \tag{2}$$

where $U_n(\mathbf{k})$ includes the nth iteration phase estimate. The equivalent of Eq. (2) in real space is:

$$u_{n+1}(\mathbf{r}) = u_n^2(\mathbf{r}) \tag{3a}$$

or

$$u_{n+1}(\mathbf{r}) = \hat{O}(u_n(\mathbf{r})), \tag{3b}$$

where $\hat{O}$ is a sharpening operator applied on a given real space potential map $u_n(\mathbf{r})$, the Fourier Transform of $U_n(\mathbf{k})$. The operator enhances strong features which may correspond to potential atom sites and minimizes weak ones. After sharpening, the FOM is calculated and the process is iterated as long as the FOM continues to decrease.

This classic Direct Methods approach has several assumptions that will preclude its straightforward application to solving surface structures. It is assumed that there are no missing strong reflections. The probability relationships on which the method is based are strongly dependent on the relative intensity of the reflections. However, in many surface diffraction patterns the bulk reflections coincide with the strongest surface reflections making them unmeasurable and leaving large holes in the data set. Another specific problem for surfaces is that the number of atoms for a particular surface structure is usually unknown. In addition, the atoms that have not been displaced far from bulk positions may well be masked in the phase map.

To overcome the problem of missing information, the Minimum Relative Entropy method uses a function similar to relative entropy as a self-consistent operator. Defining the relative entropy as:

$$\begin{aligned} &S_r(\mathbf{r}) = u(\mathbf{r}) ln[u(\mathbf{r})/e\langle u(\mathbf{r})\rangle] + \langle u(\mathbf{r})\rangle, \qquad u(\mathbf{r}) > 0, \\ &S_r(\mathbf{r}) = 0, \qquad u(\mathbf{r}) < 0, \end{aligned} \tag{4}$$

where $\langle u(\mathbf{r})\rangle$ is the mean value of $u(\mathbf{r})$, the maximum information case is attained for $u(\mathbf{r}) = \langle u(\mathbf{r})\rangle$ which minimizes to zero $S_r(\mathbf{r})$. An operator based on Eq. (4) provides an interpolation of the unmeasured reflections and Eqs. (3a) and (3b) becomes:

$$u_{n+1}(\mathbf{r}) = u_n(\mathbf{r}) ln[u_n(\mathbf{r})/\langle u_n(\mathbf{r})\rangle]. \tag{5}$$

The application of this operator to a surface potential/charge density map reduces the background noise, minimizing it in the real space phase maps and favors ''peaks'' which would correspond to potential atom sites.

To account for the finite number of reflections in a data set due to the measured intensities not extending to infinity, the unitary structure factors are modified by a window function:

$$U^{\text{new}}(\mathbf{k}) = W(\mathbf{k}) U^{\text{old}}(\mathbf{k}) \tag{6}$$

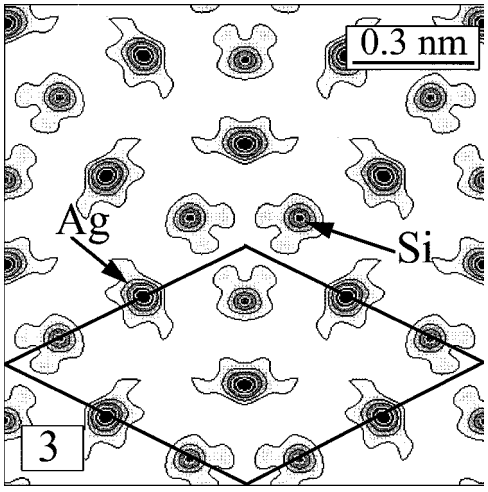

Fig. 3. Contour map of the scattering potential found for Si(1 1 1)-($\sqrt{3}\times\sqrt{3}$)R30°Ag. One (out of the three symmetry equivalent) site is arrowed for Ag and Si respectively. The primitive unit cell is indicated by solid lines. Scale bar indicates 0.3 nm.

chosen to satisfy in real space the equation ($w(\mathbf{r})$ being the Fourier Transform of $W(\mathbf{k})$):

$$w(\mathbf{r}) = \alpha w(\mathbf{r}) ln[w(\mathbf{r})/\langle w(\mathbf{r})\rangle], \quad (7)$$

where α is a constant. The window function can be considered as giving any single non-overlapping atom a relative entropy value of zero. The FOM utilized is selected as a measure of how close the relative entropy is to zero for the experimental reflections:

$$\text{FOM} = \sum{}' |U_n(\mathbf{k}) - \beta U_{n+1}(\mathbf{k})| / \sum{}' |U_n(\mathbf{k})|, \quad (8)$$

where $\sum'$ is a sum excluding $\mathbf{k} = \mathbf{0}$ and β is a scalar chosen to minimize FOM. Since the experimental data set is not perfect, having non-zero errors and the measured reflections not extending to infinity, a low FOM will correspond only to a plausible solution. However, a low FOM is a necessary condition for a correct solution.

4.1. Genetic algorithm

Since the surface diffraction patterns are usually incomplete and noisy, there may be several possible local minima in the solution space requiring the use of a global search routine, such as a genetic algorithm. In the present method, the genetic algorithm is utilized mostly for the exploration of the possible unique solutions instead of looking for a single best solution.

Initially, phases are assigned randomly for a subset of the strongest reflections, usually 5%–15% of the total number of beams. This set of starting phases is generated a total of **N** times, making a collection later referred to as a ''population''. For each starting set of phases (initial guess) the phases of the remaining reflections are calculated using the Minimum Relative Entropy method and a corresponding FOM is calculated. The assigned phases of the reflections from the subset are then translated into binary notation and strung end-to-end to create a single string of bits or a ''chromosome''. Each chromosome will be considered with its associated FOM.

The genetic algorithm will act upon the chromosomes simulating a process of natural selection, for more details see Goldberg (1989). The initial set of chromosomes will be considered as the first set of ''parent'' chromosomes. Using the value of the FOM as a likelihood for survival, the genetic algorithm selects two favorable (low FOM) parents, switches a random number of phases between them (''cross-over'') generating two new guesses or ''children'' for the starting phases, and introduces a degree of mutation in which the values of some of the phases are randomly changed. A number of parents with low FOM are just copied to the new population, an elitism process preserving the best solutions. Thus a new population corresponding to a new set of plausible solutions evolves and is subsequently evaluated and assigned a FOM through Minimum Relative Entropy. The entire process is iterated for a given number of cycles or ''generations''.

The efficiency of the genetic algorithm as a global search technique is due to the large number of schemata calculated and its specific way of processing them (Holland, 1975). A schemata is a similarity template describing a subset of chromosomes with similarities at certain positions, similar to phase combinations for different structure factors. Even for the case when the number of parents is the same as the number of children **N**, the algorithm processes around $\mathbf{N}^3$ schemata. Shorter schemata are favored and passed along each generation as cross-over disrupts longer schemata by occurring within their length. Schemata being the equivalent to favorable phase combinations, good combinations will be targeted and preserved.

4.2. Initial models and refinement

The only pieces of information fed into the Direct Methods analysis are the experimental intensities and an assumption about the structure symmetry. The output is a list of plausible solutions, phase maps obeying the imposed symmetry, ranked in order of FOM and used as a starting point for constructing possible models of the surface structure. These maps can be rather accurate restorations of the scattering potential/two-dimensional charge density (electron/X-ray data) provided the data set has small experimental measurements errors, is complete, and not affected by non-kinematical scattering. If this is the case, the bright circular features displayed in the phase maps can be interpreted as atom sites as the projection of the charge density around individual atoms can be approximated as being circular. However, the missing information that often characterizes experimental data sets will induce distortions of features' shapes as well as artifacts.

In effect, with no additional information other than the symmetry group and the beam intensities, one has limited

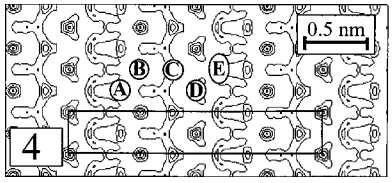

Fig. 4. Contour map of the scattering potential found for Si(1 1 1)-(3 × 1) Ag. Peaks A, B, C and D correspond to Si atoms and peak E corresponds to two half-occupancy Ag sites. A centered 6 × 1 unit cell is drawn showing the cm symmetry. Scale bar indicates 0.5 nm.

the number of solutions from an infinite number of possible arrangements of atoms to some finite number of solutions. These solutions can be further discriminated by a χ^2 minimization and comparison with results from other surface sensitive techniques.

Fig. 3 shows the phase map generated for the known Si(1 1 1)-($\sqrt{3} \times \sqrt{3}$)R30°Ag structure (electron data). Both Ag and Si sites are very well resolved, circular in shape, and no artifacts are present. For Si(1 1 1)-(3 × 1)Ag, the potential map shown in Fig. 4 displays four well-resolved peaks (A–D) along with an elongated area labeled E. The region E was considered to represent either two partially-occupied atom sites or an artifact arising from the lack of a complete set of intensities. Fig. 5 shows the electron density map obtained from X-ray data taken from the Ge(1 1 1)-(4 × 4)Ag surface. All the atom sites are well resolved, but due to the relatively similar scattering factors of Ag and Ge it is not clear which sites are occupied by Ag and which are occupied by Ge. Sometimes only part of the surface structure can be identified in the phasing map. Fig. 6(a) shows an initial fragment of Si(1 1 1)-(6 × 6)Au reconstruction with twenty Au positions and three weaker Si sites.

To complete the structure or to solve the problems raised by maps such as the ones from Figs. 4 and 5, a new step in the analysis is performed. Iterative steps of refinement of the atomic positions are combined with heavy-atom holography to determine new sites. Cross-correlation of a phasing map for a single atom with the phase map generated by Direct Methods produces a new map, highlighting the atomic positions within the unit cell. After a minor refinement (R-factor type) of the atomic positions, new possible atomic sites are generated using a heavy-atom holography algorithm. This algorithm includes a diffraction pattern fitting, providing an evaluation of the effect of placing a new atom in a suggested site. In the example from Fig. 4, the area E was finally modeled as two half-occupied Ag sites, and the A–D sites as being Si atom positions. From the map shown in Fig. 5, many different permutations of the Ag and Ge atoms distributed on the well-resolved atomic sites were tested to find the model yielding the lowest R-factor. Fig. 6(b)–(d) shows intermediate steps and the final gold framework for the Si(1 1 1)-(6 × 6)Au model.

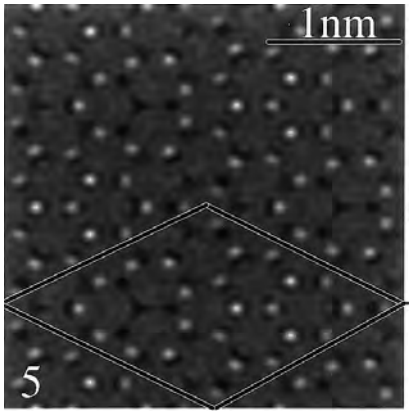

Fig. 5. Phase map calculated by Direct Methods showing the best solution for Ge(1 1 1)-(4 × 4)Ag. The primitive unit cell is indicated by solid lines. Scale bar indicates 1 nm.

As a final step, the model's atomic positions are refined using usually a reduced χ^2 minimization (Bevington, 1969), $n = 2$ in Eq. (9):

$$\chi^n = \frac{1}{N-m} \sum_{j=1}^{N} \left(\left| I^j_{\text{expt}} - I^j_{\text{calc}} \right| \Big/ \sigma^j \right)^n, \tag{9}$$

where $I_{\text{expt/calc}}$ is the experimental/calculated beam intensity, σ the error of the measured intensity, N the number of data points, and m the number of parameters being fit. For a perfect fit of the model to the measured beam intensities within the experimental uncertainty, the χ^2 value should approach 1. The χ^2 analysis assumes Gaussian distributed errors between the measurements and the simulations. For the case of exponentially distributed errors, a more robust form χ can be used ($n = 1$ in Eq. (9)). The χ factor is analogous to a χ^2 analysis, since a good fit of the model is equivalent to a value of χ near 1, but it is less sensitive to outliers in the data set.

5. Discussion

The application of Direct Methods to solve surface reconstructions is a new area which will continue to grow in scope and magnitude in the near future. The major differences between bulk and surface diffraction data that precluded the application of Direct Methods to surface determination have been overcome. In particular, this technique has proven useful not only as an interpolation tool for estimating unmeasured reflections, but also as an instrument for extrapolating information to higher spatial frequencies. In principle, this method offers the possibility of estimating intensities from beam reflections which coincide with bulk or 1 × 1 lattice intensities, information which has mostly gone unused or ignored.

Areas which require further development are cases of the surfaces where twinning is present or large structures where only an initial fragment is present in the phase maps. In the latter case, often the final model obtained after the heavy-atom holography method is path dependent requiring careful process monitoring. Hence a more automated method is

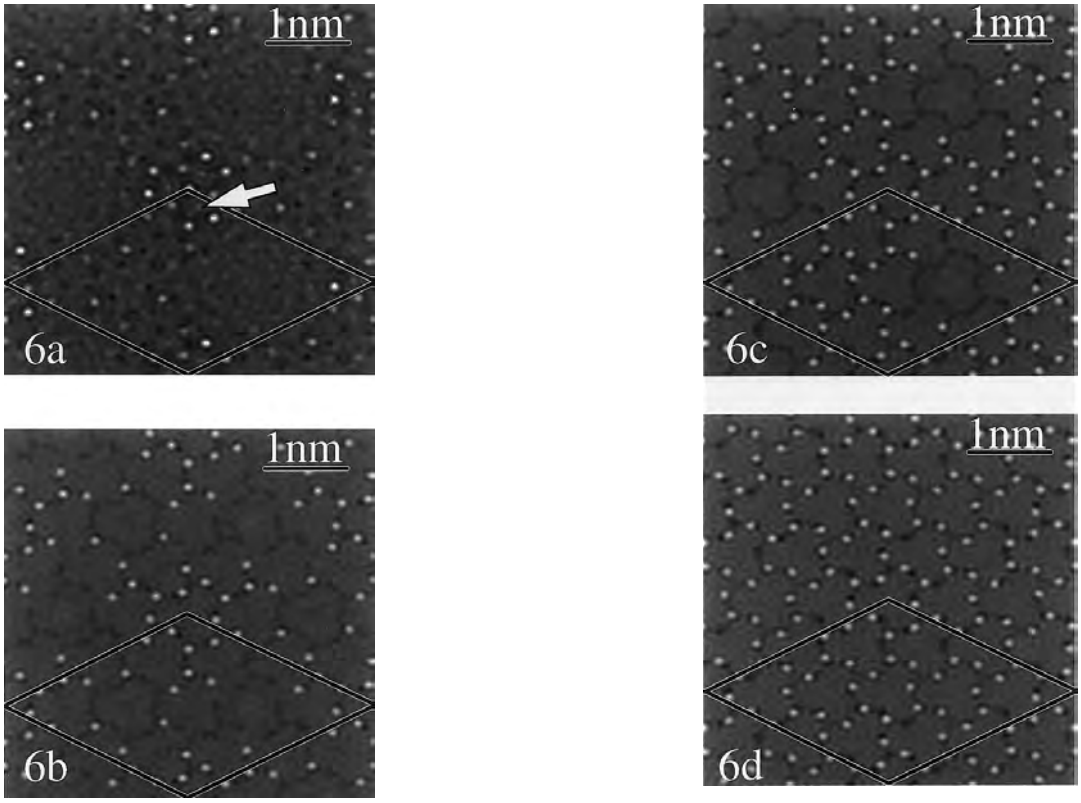

Fig. 6. (a) Phase map calculated by Direct Methods showing an initial fragment of the Si(1 1 1)-(6 × 6)Au. A weaker Si site (one of the three symmetry equivalent) is arrowed, all the other peaks correspond to Au sites. (b) and (c) intermediate steps in constructing the atomic model; (d) final model for the Au atoms. The primitive unit cell is indicated by solid lines. Scale bar indicates 1 nm.

desired. More interesting, the extension of the Direct Methods analysis to three-dimensional diffraction surface data (including the rel-rod information from X-ray surface diffraction measurements) is under investigation and already shows some degree of success.

The improvement of the quality of information obtained from HREM imaging is currently being addressed in our group through replacing the present TV-rate CCD camera with a slow-scan CCD one. More importantly, an on-line Wiener filter is being installed, which will reduce the noise level and provide real-time image enhancement. This will also allow us to monitor the microscope aberrations, and therefore achieve a more accurate correction, greatly improving the image acquisition and analysis capabilities. Higher brightness instruments using field emission electron gun sources will also lead to improvements.

In the future, progress in both HREM imaging and Direct Methods has the potential to open the way for significant advances in even more challenging areas of research, such as solving the structure of buried interfaces (which by their nature are not accessible to almost all other surface probes), and investigating chemical reactions on reconstructed surfaces.

This is not to suggest that HREM and Direct Methods will be the only tools in surface characterization. Up to date both techniques are only weakly sensitive to chemical composition or specific chemical bonding information. Nonetheless, these methods offer powerful tools which, when combined with other surface characterization techniques, can give a complete and accurate view of the surface structure.

Acknowledgements

We would like to acknowledge the support of the National Science Foundation on grant #DMR-92114505.

References

Bengu, E., Plass, R., Marks, L.D., Ichihashi, T., Ajayan, P.M., Iijima, S., 1996. Imaging the dimers in Si(1 1 1)-(7 × 7). Phys. Rev. Lett. 77, 4226–4228.

Bevington, P.R., 1969. Data Reduction and Error Analysis for the Physical Sciences. McGraw-Hill, New York.

Binning, G., Rohrer, H., 1987. Scanning tunneling microscopy – from birth to adolescence. Rev. Mod. Phys. 59, 615–627.

Collazo-Davila, C., Grozea, D., Landree, E., Marks, L.D., 1997a. Transmission electron diffraction determination of the Ge(0 0 1)-(2 × 1) surface structure. Surf. Sci. 375, 293–301.

Collazo-Davila, C., Grozea, D., Marks, L.D., 1998. Determination and refinement of the Ag/Si(1 1 1)-(3 × 1) surface structure. Phys. Rev. Lett. 80, 1678–1681.

Collazo-Davila, C., Grozea, D., Marks, L.D., Feidenhans'l, R., Nielsen, M.,

Seehofer, L., Lottermoser, L., Falkenberg, G., Johnson, R.L., Gothelid, M., Karlsson, U., 1998b. Direct Methods solution of the Ge(1 1)-(4 × 4)Ag surface. Surf. Sci. 418, 395–406.

Collazo-Davila, C., Marks, L.D., Nishii, K., Tanishiro, Y., 1997b. Atomic structure of the In on Si(1 1 1)-(4 × 1) surface. Surf. Rev. and Lett. 4, 65–70.

Diamon, H., Chung, C., Ino, S., Watanabe, Y., 1990. A study of Si(1 1 1)5 × 2-Au structures by Li adsorption and their coadsorbed superstructures. Surf. Sci. 235, 142–155.

Dorset, D.L., 1995. Structural Electron Crystallography. Plenum Press, New York.

Erwin, S.C., 1995. New structural model for the alkali-induced Si(1 1 1)-(3 × 1) reconstruction from first principles. Phys. Rev. Lett. 75, 1973–1976.

Giacovazzo, C., 1980. Direct Methods in Crystallography. Plenum Press, New York.

Gilmore, C.J., Marks, L.D., Grozea, D., Collazo-Davila, C., Landree, E., Twesten, R.D., 1997. Direct solutions of the Si(1 1 1) 7 × 7 structure. Surf. Sci. 381, 77–91.

Goldberg, D.E., 1989. Genetic Algorithms in Search, Optimization and Machine Language. Addison-Wesley, New York.

Hasegawa, T., Takata, K., Hosaka, S., Hosoki, S., 1991. Initial stage of Au adsorption onto a Si(1 1 1) surface studied by scanning tunneling microscopy. J. Vac. Sci. Technol. B 9, 758–761.

Hasegawa, T., Hosaka, S., Hosoki, S., 1992. In situ observation of gold adsorption onto Si(1 1 1) 7 × 7 surface by scanning tunneling microscopy. Jap. J. Appl. Phys. 31, L1492–L1494.

Hasegawa, T., Takata, K., Hosaka, S., Hosoki, S., 1996. Domain growth of Si(1 1 1)-5 × 2 Au adsorption by high temperature STM. Surf. Sci. 357, 858–862.

Holland, J.H., 1975. Adaptation in Natural and Artificial Systems. University of Michigan Press, Ann Arbor.

Krakow, W., 1982. The direct observation of atomic surface structure and inclined planar defects in Au (1 1 1) films. Thin Solid Films 93, 235–253.

Landree, E., Collazo-Davila, C., Marks, L.D., 1997. A multi-solution genetic algorithm approach to surface structure determination using Direct Methods. Acta Cryst. B 53, 916–922.

Landree, E., Marks, L.D., Zschack, P., Gilmore, C.J., 1998. Structure of the TiO_{2-x}(1 0 0)-1 × 3 surface by Direct Methods. Surf. Sci. 408, 300–309.

Lu, P., Smith, D.J., 1991. Direct imaging of CdTe(0 0 1) surface reconstructions by high-resolution electron microscopy. Surf. Sci. 254, 119–124.

Marks, L.D., 1983. Direct imaging of carbon-coated and clean gold (1 1 0) surfaces. Phys. Rev. Lett. 51, 1000–1002.

Marks, L.D., 1996. Wiener-filter enhancement of noisy HREM images. Ultramicroscopy 62, 43–52.

Marks, L.D., Bengu, E., Collazo-Davila, C., Grozea, D., Landree, L., Leslie, C., Sinkler, W., 1998a. Direct Methods for surfaces. Surf. Rev. and Lett. 5, 1087–1106.

Marks, L.D., Grozea, D., Feidenhans'l, R., Nielsen, M., Johnson, R.L., 1998b. Au 6 × 6 on Si(1 1 1): evidence for a 2-D pseudo glass. Surf. Rev. and Lett. 5, 459–464.

Marks, L.D., Landree, E., 1998. A minimum entropy algorithm for surface phasing problems. Acta Cryst. A 54, 296–305.

Marks, L.D., Plass, R., 1995. Atomic structure of Si(1 1 1)-(5 × 2)-Au from high resolution electron microscopy and heavy-atom holography. Phys. Rev. Lett. 75, 2172–2175.

Marks, L.D., Plass, R., Dorset, D., 1997. Imaging surface structures by direct phasing. Surf. Rev. and Lett. 4, 1–8.

Marks, L.D., Smith, D.J., 1983. Direct surface imaging in small metal particles. Nature 303, 316–317.

Marks, L.D., Xu, P., Dunn, D.N., 1993. UHV transmission electron microscopy of Ir(0 0 1). II Atomic positions of the (5 × 1) reconstructed surface from HREM and R-factor refinements. Surf. Sci. 294, 322–332.

Minoda, H., Tanishiro, Y., Yamamoto, N., Yagi, N., 1992. Growth of a Si on Au deposited Si(1 1 1) surfaces studied by UHV-REM. Appl. Surf. Sci. 60, 107–111.

Nihoul, G., Abdelmoula, K., Métois, J.J., 1984. High resolution images of a reconstructed surface structure on (1 1 1) gold platelets: interpretation and comparison with theoretical models. Ultramicroscopy 12, 353–366.

Plass, R., Marks, L.D., 1995. UHV transmission electron microscopy structure determination of the Si(1 1 1)-($\sqrt{3} \times \sqrt{3}$)R30°Au surface. Surf. Sci. 342, 233–249.

Plass, R., Marks, L.D., 1997. Submonolayer Au on Si(1 1 1) phase diagram. Surf. Sci. 380, 497–506.

Plass, R., Egan, K., Collazo-Davila, C., Grozea, D., Landree, E., Marks, L.D., Gajdardziska-Josifovska, M., 1998. Cyclic ozone identified in magnesium oxide (1 1 1) surface reconstructions. Phys. Rev. Lett. 81, 4891–4894.

Shibata, A., Kimura, Y., Takayanagi, K., 1992. Si(1 1 1)-($\sqrt{3} \times \sqrt{3}$)-Au growing on a 7 × 7 surface. Surf. Sci. 273, L430–L434.

Swiech, W., Bauer, E., Mundschau, M., 1991. A low-energy electron microscopy study of the system Si(1 1 1)-Au. Surf. Sci. 253, 283–296.

Takahashi, S., Tanishiro, Y., Takayanagi, K., 1991. Short range orders of an adsorbed layer: gold on the Si(1 1 1)-7 × 7 surface. Surf. Sci. 242, 73–80.

Tanishiro, Y., Takayanagi, K., 1989a. Validity of the kinematical approximation in transmission electron diffraction for the analysis of surface structures. Ultramicroscopy 27, 1–8.

Tanishiro, Y., Takayanagi, K., 1989b. Dynamic observation of gold adsorption on Si(1 1 1)-7 × 7 surface by high-resolution reflection electron microscopy. Ultramicroscopy 31, 20–28.

Weitering, H.H., DiNardo, N.J., Pérez-Sandoz, R., Chen, J., Mele, E.J., 1994. Structural model for the metal-induced Si(1 1 1)3 × 1 reconstruction. Phys. Rev. B 49, 16837–16840.

Wood, E.A., 1964. Vocabulary of surface crystallography. J. Appl. Phys. 35, 1306–1311.

Woolfson, M.M., 1987. Direct Methods – from birth to maturity. Acta Cryst. A 43, 593–612.

Woolfson, M.M., Fan, H.-F., 1995. Physical and Non-physical Methods of Solving Crystal Structures. Cambridge University Press, Cambridge, London.

Xu, P., Dunn, D.N., Zhang, J.P., Marks, L.D., 1993. Atomic imaging of surfaces in plan view. Surf. Sci. 285, L479–L485.

Xu, P., Jayaram, G., Marks, L.D., 1994. Cross-correlation method for intensity measurement of transmission electron diffraction patterns. Ultramicroscopy 53, 15–18.

Xu, P., Marks, L.D., 1992. Intensities of surface diffraction spots in plan view. Ultramicroscopy 45, 155–157.

Yuhara, J., Inoue, M., Morita, K., 1992a. Phase transition of the Si(1 1 1)-Au surface from $\sqrt{3} \times \sqrt{3}$to 5 × 1 structure studied by means of the low-energy electron diffraction, Auger electron spectroscopy, and Rutherford backscattering spectroscopy techniques. J. Vac. Technol. A 10, 334–338.

Yuhara, J., Inoue, M., Morita, K., 1992b. Commensurate-incommensurate phase transition between 6 × 6 and $\sqrt{3} \times \sqrt{3}$ + satellite structures of the Si(1 1)-Au surface. J. Vac. Technol. A 10, 3386–3492.